FOURTH EUROPEAN ROTORCRAFT AND POWERED LIFT AIRCRAFT FORUM

Paper No 2

# THE PREDICTION OF SUPERCRITICAL PRESSURE DISTRIBUTIONS ON BLADE TIPS OF ARBITRARY SHAPE OVER A RANGE OF ADVANCING BLADE AZIMUTH ANGLES

J GRANT
Royal Aircraft Establishment
England

September 13 - 15 1978
STRESA - ITALY

Associazione Italiana di Aeronautica ed Astronautica
Associazione Industrie Aerospaziati

# THE PREDICTION OF SUPERCRITICAL PRESSURE DISTRIBUTIONS ON BLADE TIPS OF ARBITRARY SHAPE OVER A RANGE OF ADVANCING BLADE AZIMUTH ANGLES

J GRANT

Royal Aircraft Establishment
England

## 1 Introduction

Following the successful development of finite-difference calculation methods for computing flows over fixed aerofoils and wings, these methods are now being applied to the important problem of helicopter blade tip aerodynamics. One particular area which is amenable to analysis is the calculation of the supercritical flow over the tip region of the blade on the advancing side of the rotor disc where, in high speed flight, strong compressible flow effects can occur which may limit high speed performance[1]. At RAE, a transonic small perturbation approximation to the equations for potential flow over a helicopter blade has been derived and a numerical technique devised to provide a three-dimensional solution for various tip shapes, at azimuth stations around the advancing side of the disc. With such a method available, a theoretical study of different tip shapes can be undertaken with a view to minimising the adverse effects of the development of supercritical flow.

In this paper, the calculation method is described and the assumptions made in deriving the flow-field equation are discussed, together with those made in related studies[2, 5]. The numerical scheme is outlined and a selection of results for different planforms is presented to illustrate the influence of three-dimensional tip effects in the azimuth range $60^{\circ}$ to $120^{\circ}$.

## 2 The Flow Equation

Exact calculation of the three-dimensional, time-dependent airflow about a helicopter blade as it moves around the rotor disc is an extremely formidable problem. Even if we ignore all blade dynamics and assume inviscid and irrotational flow, so that the air velocity can be derived from a perturbation potential $\phi$, we are confronted by field equations (Ref 3, eqns (2.1) and (2.2)) which have so far defied analysis. Progress can be made, however, towards calculating the supercritical flow relative to the blade on the advancing side of the rotor disc by applying a transonic small perturbation (tsp) approximation, as in the manner of Ref 4 for example.

In previous studies of the advancing blade problem[2, 5, 6] it has been chosen to ignore the spanwise component of freestream velocity along the blade in comparison with the chordwise component. Of course at $90^{\circ}$ azimuth, where the rotational velocity and the air velocity due to the forward motion are both in the chordwise direction, this is certainly acceptable. Away from $90^{\circ}$ azimuth, however, the spanwise component of the flow can be expected to have an appreciable effect, especially for large advance ratios, and even for low advance ratios if swept tips are to be examined. Thus if the flow is to be considered over a range of azimuth angle, spanwise flow effects should be accounted for. Assuming then that in general the spanwise component of the flow is of the same order as the chordwise component, for a helicopter with forward velocity $U$, rotor of radius $R$ and blades of chordlength $c$ rotating with angular velocity $\Omega$, we derive[3] the following tsp equation in the velocity perturbation potential $\phi$ to describe the motion:

$$\phi_{xx}\left[1 - M_T^2U_1^2 - (\gamma + 1)M_T^2U_1\phi_x - (\gamma - 1)M_T^2U_2\phi_y\right]$$

$$+ \phi_{yy}\left[1 - M_T^2U_2^2 - (\gamma - 1)M_T^2U_1\phi_x - (\gamma +)M_T^2U_2\phi_y\right]$$

$$- 2\phi_{xy}\left[M_T^2U_1U_2 + M_T^2U_1\phi_y + M_T^2U_2\phi_x\right]$$

$$+ \phi_{zz}\left[1 - (\gamma - 1)M_T^2\ U_1\phi_x + U_2\phi_y\right)\Big]$$

$$- 2M_T^2U_1\phi_z\ \phi_{xz} - 2M_T^2\ \phi_z\ \phi_{yz}$$

$$- \frac{1}{A}M_T^2\ \left(U_2 + \mu\ \cos\Psi\right)\phi_x + \frac{1}{A}M_T^2\ \left(U_1 + \mu\ \sin\Psi\right)\phi_y$$

$$- \frac{2}{A}M_T^2\ U_1\ \phi x\Psi\ - \frac{2}{A}M_T^2U_2\ \phi y\Psi \qquad = 0 \qquad (2.1)$$

where

$$U_1 = \frac{A_I + \gamma}{A} + \mu\ \sin\ \Psi \quad ,$$

$$U_2 = -\frac{(x + \frac{1}{4})}{A}\ \mu\ \cos\ \Psi \quad ,$$

$$A_I = (R - I)/c \quad ,$$

and $M_T$ $(= \Omega R/a_\infty)$ is the blade tip Mach number due to rotation, $\mu$ $(= U/\Omega R)$ is the helicopter advance ratio and $A(= R/c)$ is the blade aspect ratio for a rectangular planform. In equation (2.1) x, y and z are space co-ordinates measured relative to axes Ox, Oy, Oz centred at the rotor hub and rotating with the blade such that Oy is along the blade, Ox is parallel to the blade chord (x increasing aft) and Oz is normal to the rotor disc as shown in Figure 1. The velocity potential $\phi$ and the space co-ordinates have been non-dimensionalised by making the substitutions

$$\phi \longrightarrow c(\Omega R)\phi$$
$$x \longrightarrow c(x + \tfrac{1}{4})$$
$$y \longrightarrow R - I + cy$$
$$z \longrightarrow cz$$

Then as illustrated in Figure 2, $x = -\frac{1}{2}$ corresponds to the blade leading edge and $x = +\frac{1}{2}$ to the blade trailing edge; $y$ is the distance in chord-lengths towards the tip from some specified inboard station I, so that near the tip $(A_I + y)/A$ is almost equal to unity. The symbols $U_1$ and $U_2$ represent the chordwise and spanwise components of velocity in terms of the non-dimensional variables.

Equation (2.1) contains terms which involve derivatives with respect to all three space co-ordinates, and also two terms which involve derivatives with respect to the azimuth angle $\psi$ and so portray the time dependent nature of the flow. Although it is much simpler than the full potential equation for the motion it would appear that no solutions to equation (2.1) have, as yet, been presented.

Isom and Caradonna in the USA have, however, in Ref 2, investigated time dependent effects for the case of a non-lifting rectangular blade with circular arc section. They did this by integrating, over a range of values of azimuth on the advancing side of the rotor disc, an equation essentially equivalent to equation (2.1) when all terms arising from the spanwise component of the flow (that is those terms involving $U_2$ in (2.1)) were neglected. Their calculations indicated that the time dependent solution did not differ significantly from a steady calculation at the same azimuth until the blade azimuth angle was well in excess of $90^\circ$.

It was felt, then, by the author that accurate calculations of the flow relative to a helicopter blade could be made over a useful range of azimuth angle about $90^\circ$, by <u>omitting</u> the two time dependent terms in equation (2.1) but <u>retaining</u> all spanwise flow terms. This would permit a 'steady' three-dimensional computation to be performed at the prescribed azimuth under consideration. It was also decided to direct some effort towards the simulation of lifting cases so that the combination of new planforms and recently developed cambered aerofoil sections could be considered together.

## 3 <u>The Numerical Method</u>

For the reasons given above, the equation which was retained for numerical analysis was of the form (2.1) <u>without</u> the last two time-dependent terms.

To set the governing equation in finite difference form poses problems, since to ensure stability in local regions where the flow is supersonic it is necessary to switch from central to upwind finite difference forms in a direction corresponding to the local velocity vector. Since the freestream flow has both chordwise and spanwise components this will obviously imply switching finite difference expressions to backward form in both the $x$ and $y$ co-ordinate directions but it is not apparent from the form of (2.1) to which terms this should apply and to which terms it should not. An answer has been

found by looking for guidance to the analogous situation of yawed flow over a fixed wing. By applying the canonical splitting scheme suggested independently by Albone[7] and Jameson[8] it has been shown by the Author[3] that the governing equation should be finite-differenced in the form

$$\underline{\left[1 - M_T^2\left(U_1^2 + U_2^2\right) - (\gamma+1)M_T^2\left(U_1\phi_x + U_2\phi_y\right)\right]\left(p_1^2\phi_{xx} + 2p_1p_2\phi_{xy} + p_2^2\phi_{yy}\right)}$$

$$+ \left[p_2^2\left\{1 - (\gamma+1)M_T^2\left(U_1\phi_x + U_2\phi_y\right)\right\} + 2M_T^2U_2\phi_y\right]\phi_{xx}$$

$$+ \left[p_1^2\left\{1 - (\gamma+1)M_T^2\left(U_1\phi_x + U_2\phi_y\right)\right\} + 2M_T^2U_1\phi_x\right]\phi_{yy}$$

$$- 2\left[p_1p_2\left\{1 - (\gamma+1)M_T^2\left(U_1\phi_x + U_2\phi_y\right)\right\} + M_T^2U_1\phi_y + M_T^2U_2\phi_x\right]\phi_{xy}$$

$$+ \left[1 - (\gamma-1)M_T^2\left(U_1\phi_x + U_2\phi_y\right)\right]\phi_{zz}$$

$$- 2M_T^2U_2\phi_z\phi_{yz} - 2M_T^2U_1\phi_z\phi_{xz}$$

$$- \frac{1}{A}M_T^2\left(U_2 + \mu\cos\psi\right)\phi_x + \frac{1}{A}M_T^2\left(U_1 + \mu\sin\psi\right)\phi_y$$

$$= 0 \qquad (2.3)$$

where

$$p_1^2 = U_1^2 / \left(U_1^2 + U_2^2\right)$$

$$p_2^2 = U_2^2 / \left(U_1^2 + U_2^2\right)$$

$$p_1p_2 = U_1U_2 / \left(U_1^2 + U_2^2\right)$$

The underlined terms in equation (2.3) are those which must be switched to backward form when the flow is supercritical. When the terms in equation (2.3) are combined they reduce to equation (2.1) (without the time-dependent terms), but in the form (2.3) it is evident that only parts of the $\phi_{xx}$, $\phi_{xy}$ and $\phi_{yy}$ terms must be switched, while other parts should remain centrally differenced everywhere.

The sonic condition for equation (2.1) is, to leading order,

$$1 - M_T^2\left(U_1^2 + U_2^2\right) - (\gamma+1)M_T^2\left(U_1\phi_x + U_2\phi_y\right) = 0$$

It can be seen from equation (2.3) that the switch from central to backward differences (where the flow becomes sonic) occurs smoothly. With regard to the y direction, 'backward' will depend upon the direction of the spanwise component of the flow, ie the sign of $U_2$. Once again a smooth switch in the y derivative terms will occur even if $U_2$ changes sign because $p_2$ (and hence $U_2$) multiplies each of these terms.

## 3.1 Boundary conditions

To complete the formulation of the problem boundary conditions must be applied - on the rotor surface, at the inboard boundary I, in the far field and on the wake. The inboard boundary station $y = o$ can be specified arbitrarily. It is taken to be sufficiently far inboard, away from tip effects, so that, if the blade is uniform, it can be assumed that there is no perturbation to the flow in the direction, n, normal to the local free-stream direction. Thus as $y \to o$, then $\phi_n \to o$ and $\phi_{nn} \to o$. In terms of the blade - based co-ordinate system this gives at $y = o$

$$U_1 \phi_y - U_2 \phi_x = 0$$

$$U_1^2 \phi_{yy} - 2U_1 U_2 \phi_{xy} + U_2^2 \phi_{xx} = 0$$

which enable the spanwise derivatives in equation (2.3) to be eliminated leaving an equation involving only x and z at $y = o$. On the rotor blade the flow tangency condition

$$\phi_z \Big|_{z = o^{\pm}} = U_1 \frac{\delta Z_s^{U/L}}{\delta x} + U_2 \frac{\delta Z_s^{U/L}}{\delta y} \qquad (2.5)$$

is enforced, where $Z_s^{U/L}$ are the co-ordinates of the upper and lower blade surfaces.

In order to treat lifting cases it is necessary to model the vortex wake. It is well known that the vortex sheet trailing from a rotor blade usually rolls up to form a strong line-vortex. For high advance ratios, however, (around the advancing side of the disc where the loading is low,) the vortex sheet appears to remain reasonably planar at least for a few chordlengths downstream. As a first approach it was decided to model the wake generated by the tip region of the blade as a plane vortex sheet skewed in the direction of the resultant freestream flow. Figure 3 illustrates the model of the wake for azimuth angles of 60° and 120°. At 60° azimuth the wake arising from the straight edge of a rectangular blade is also taken into account. Across the vortex sheet, jump conditions on the velocity potential are imposed. To the leading order, to obtain continuity of pressure we must ensure that $\phi_s$ is continuous across the vortex sheet, where s is in the direction of the local velocity vector. This in turn implies that $(\Delta\phi)_s = 0$, where $\Delta\phi$ is the potential jump across the sheet. This jump condition is imposed in the course of the numerical solution.

With regard to the far field conditions, we assume that in a Trefftz plane far downstream of the aerofoil the pressure will have recovered to the appropriate freestream value. In this case $\phi_s \rightarrow 0$ and $\phi_{ss} \rightarrow 0$, which implies

$$U_1\phi_x + U_2\phi_y = 0$$

$$\left(U_1 \frac{\partial}{\partial x} + U_2 \frac{\partial}{\partial y}\right)\left(U_1\phi_x + U_2\phi_y\right) = 0 \qquad (2.6)$$

The conditions (2.6) enable all $x$ derivative terms in (2.3) to be eliminated leaving an equation in only $y$ and $z$, which is solved in the Trefftz plane downstream. At any particular azimuth under consideration, the spiral wake, blade dynamics and blade twist can be accounted for approximately by performing computations for an effective incidence distribution, which has been obtained previously from a complete rotor performance calculation which does model these effects. Though there are uncertainties concerning the true incidence distribution in any situation, it can be reasoned that as blade incidence varies with advance ratio, what is required is a blade tip which performs well for a range of incidence distributions. Leaving this question for debate, what we can assert more confidently is that the theory outlined should give reasonable results for cambered sections at near zero lift.

Once the scheme indicated by equation (2.3) to (2.6) has been established the finite difference solution of the equations follows the same lines as in many other finite difference methods and is described in Ref 6 and 9. The method which can cope with arbitrary geometry has been used to compute flows over a variety of tip shapes and for a number of aerofoil sections over a range of azimuth angles. So far no serious problems of numerical instability have been encountered. A selection of the computed results are presented below.

## 4 Comparison of Theory with Experiment

A model rotor experiment is described in Ref 10 and 11 in which detailed pressure monitoring was carried out at ONERA on untwisted blades fitted with straight and 30° sheared tips, under non-lifting conditions. Various pressure distributions over the tip region have been presented in these papers for both types of blade tip and these provide a useful means of assessing the current theory.

The first tip shown in Figure 4 was near-rectangular but was tapered in thickness from NACA 0014.5 section at 80% radius to NACA 0009 section at the tip. Pressures were monitored at the three spanwise stations indicated in Figure 4. As the blades were of low aspect ratio (~6) tip effects should extend over an appreciable extent of the blade[1]. Also as the advance ratio in the tests was high ($\mu = 0.55$) time dependent effects should be appreciable. Two-dimensional time-dependent calculation methods[10, 12] have also been used to predict the local unsteady flow at the three spanwise stations shown in Figure 4, for the time-varying chordwise component of the freestream flow. Thus comparisons between experiment and the three-dimensional and unsteady two-dimensional theories provide useful information regarding the importance of three-dimensional and unsteady effects.

Figures 5 to 8 show a three-dimensional picture of the measured and calculated pressure distributions over the tip region at 60° and 120° azimuth for the case $M_T = 0.6$, $\mu = 0.55$. At both azimuth stations the agreement is quite good, in terms of both shock pattern and pressure levels along the blade. The significant differences in the flow at 60° and 120° are captured well by the 'steady' three-dimensional theory and evidently are not due entirely to unsteady effects. Indeed the flow patterns appear to be consistent with previous observations on flows over swept back and swept forward wings, and have been interpreted in this sense in Ref 9.

The asymmetries in the flow before and beyond 90° azimuth are best illustrated by examining azimuthal variation of pressure at various points on the blade. This azimuthal variation of pressure at 30% and 50% chord at each of the two spanwise stations $r/R = 0.855$ and $r/R = 0.892$ are plotted in Figures 9 and 10, while Figure 11 shows the result at 40% chord at the most outboard radial station $r/R = 0.946$. Separate curves giving the measured variation, and that predicted by the present theory and by two-dimensional time-dependent theory have been drawn. To plot these figures for the three-dimensional case a separate steady flow result, as given by (2.3), was obtained at azimuth intervals of $7\frac{1}{2}^{\circ}$. The calculations were carried out on a fairly coarse grid consisting of 31 x 23 x 11 points in the chordwise, spanwise and normal directions.

In each of Figures 9 to 11 the flow asymmetry about $\psi = 90^{\circ}$ is very apparent, but the pressures are predicted well at all three spanwise stations by the three-dimensional theory in the azimuth interval 60° to 120°, in which range the furthest penetration into supercritical conditions occurs. Beyond 120° azimuth the distinct differences which occur between the three-dimensional and the measured pressures have been attributed to time dependent effects, an assertion which is substantiated by the very close agreement between two-dimensional unsteady theory and experiment at the most inboard radial station (Figure 9) over the whole azimuth range shown. At this inboard spanwise station tip effects are likely to be small. Towards the tip, however, the two-dimensional theory fails and at the most outboard station (Figure 11) even the trend with azimuth is not correct. The three-dimensional theory, which includes tip effects, predicts the trend well in the azimuth range 60° to 120° before once again, beyond this azimuth, time-dependent effects come into play.

The importance of three-dimensional effects (and in particular the essential role of the spanwise component of the flow) is portrayed even more strongly in the results for the ONERA model rotor when fitted with the swept tip shown in Figure 12. The tip is sheared sharply at an angle of 30° over the outer 15% of the blade and it has the same section and is tapered in thickness in the same way as for the near-rectangular tip. The pressure distribution over the tip region at 60° azimuth and 120° azimuth, as measured and as calculated by the three-dimensional theory are presented in Figures 13 and 14 respectively. Here the agreement between experiment and the calculations, which were performed on a 61 x 45 x 21 grid, is considered very good. The computations capture the high suction peak which occurs towards the sharp leading-edge corner at the extreme tip of such a sheared back blade at 60° azimuth, and the strong shock which appears at 120° azimuth where the effect of sweepback is a minimum.

It is apparent by comparing the calculated results at 60° and 120° azimuth, both for the rectangular tip and the swept tip, that there is a noticeable influence of the spanwise component of the flow even at radial stations

which are an appreciable distance inboard from the tip. This may seem surprising but perhaps can be explained by reference to Figure 15 where the resultant flow relative to the blade is shown, for a forward flight case, at 60° and 120° azimuth. As is indicated, if the same section normal to the leading edge is considered, at 60° azimuth the flow over the rear part of the section originates with freestream Mach number $M - \Delta M$ whereas at 120° azimuth the flow over the rear part of the section originates with freestream Mach number $M + \Delta M$. Of course, if the spanwise component of the flow is ignored there is no distinction between the freestream flow in each case. If, for a swept tip, spanwise (or more accurately, radial) flow terms are neglected then the Mach number normal to the swept leading-edge is the same at $\psi = 90 + \Delta\psi$ as at $\psi = 90 - \Delta\psi$. This is obviously not true in forward flight and will clearly lead to errors in the predicted pressure distributions. Figure 16, which shows the calculated spanwise variation of the chordwise maximum of the local Mach number of the flow over the swept-tip blade at 60° and 120°, illustrates that there is a measurable effect due to spanwise flow even two chordlengths from the tip.

The inability of a three-dimensional theory which neglects spanwise flow effects to predict useful results for the swept tip case is illustrated by including in Figure 16 the calculated result (the same at 60° and 120°) when all spanwise ($U_2$) terms in (2.3) are dropped.

## 5 Possible Refinements to a Swept Tip

The adverse high suction peak which appears at 60° azimuth for a rectangular blade, and also at 90° azimuth on a swept tip with a straight edge at the extreme tip, can be alleviated by rounding the leading edge corner. The theory has been used to predict the pressure distribution at 60°, 90° and 120° for a tip planform of this type. The modelled blade was sheared at an angle of 30° two chordlengths from the tip and constant NACA 0012 section was maintained over the tip region. The calculated isobar distribution over the tip is plotted in Figure 17 for the case $M_T = 0.63$, $\mu = 0.4$, $R/c = 15$, $\alpha = 0°$, $\psi = 90°$, and this may be compared with that computed for the same tip when the leading edge corner is not rounded, which is shown in Figure 18. The high suction peak at the leading edge corner has been completely eliminated. The extent of supercritical flow for this tip at 60°, 90° and 120° azimuth is illustrated in Figure 19, where the calculated variation of maximum local Mach number along the blade has been plotted. Once again this may be compared with that computed for a rectangular blade with the same section and aspect ratio, shown in Figure 20. It can be noted that at 120° azimuth, where, for the sheared tip, the benefits of sweep are the least, a higher level of supercritical flow is predicted for the sheared tip than for the rectangular tip. A similar effect has been observed in the ONERA experiments[11].

If we refer again to Figures 17 and 19 for the sheared tip, it can be seen that the sharp crank where the shearing begins produces an equally sharp decrease in local surface velocities. Such a sudden decrease in local velocity has no special merit and can be avoided with a progressively sheared tip as drawn in Figure 21. The planform of this tip was selected with the aid of the theory and the predicted levels of supercritical velocity along the blade for this shape are presented in Figure 22. The sharp drop in surface velocity at the crank is avoided without any increase in overall levels compared to the sharply sheared tip. Once again though, a significant excursion into supercritical conditions occurs at 120°. We note that for this planform the trailing edge at

the tip is only 0.88 chordlength behind the trailing edge of the inboard part of the blade as against 1.15 chordlengths for the sharply sheared blade of Figure 16. This should lead to considerably less mass behind the elastic axis of the blade.

Finally as an example of the use of the calculation method for a lifting case, chordwise pressure distributions at various radial stations on a Lynx blade, which has RAE 9615 section, are shown in Figure 23 at 90° azimuth, for the incidence distribution indicated. This incidence variation was taken from a rotor performance calculation for the flight condition $M_T = 0.63$, $\mu = 0.4$.

## 6 Conclusions

1 A method has been developed for calculating lifting three-dimensional supercritical flow over a rotor blade at arbitrary azimuth, on the advancing side of a rotor disc, by extending tsp theory to include spanwise flow terms whilst still neglecting time-dependent terms.

2 Comparisons with experimental results for a non-lifting model rotor fitted with near-rectangular and swept tip blades show good agreement over the tip region in the azimuth range 60° to 120°.

3 Beyond 120° azimuth, in highly supercritical conditions, strong time-dependent effects are apparent which the present three-dimensional theory can not predict. The unsteady effects are, however, captured well at stations some way inboard from the tip by two-dimensional time-dependent tsp theory.

4 In order to predict both three-dimensional and unsteady effects a three-dimensional time-dependent theory is required. It is advocated that the tsp equation given by (2.1) should serve well for this purpose.

5 On the basis of the calculations presented in this paper it is suggested that a progressively sheared tip with a rounded leading edge corner at the extreme tip should be effective in alleviating supercritical conditions around a large portion of the advancing side of a rotor disc.

## References


1 P G Wilby, J Grant. Transonic aerodynamics and the helicopter rotor. Paper presented at Symposium Transsonicum II, Gottingen, September 1975.

2 F X Caradonna, M P Isom. Numerical calculation of unsteady transonic potential flow over helicopter rotor blades. AIAA Journal, 14, No 4 (1976).

3 J Grant. Calculation of the supercritical flow over the tip region of a non-lifting rotor blade at arbitrary azimuth. RAE TR 77180 (1977).

4 M G Hall, M C P Firmin. Recent developments in methods for calculating transonic flows over wings. 9th Congress of the International Council of the Aeronautical Sciences (1974).

5 F X Caradonna, M P Isom. Subsonic and transonic potential flow over helicopter rotor blades. AIAA Journal, 10, No 12 (1972).

6 J Grant. Numerical prediction of the supercritical pressure distribution over the tip region of a 'non-lifting rotor blade of arbitrary tip geometry. Unpublished MOD(PE) report.

7 C M Albone. A finite-difference scheme for computing supercritical flows in arbitrary co-ordinate systems. RAE TR 74090 (1974). Also ARC CP No 1313.

8 A Jameson. Transonic potential flow calculations using conservation form. AIAA 2nd Computational Fluid Dynamics Conference (1975).

9 J Grant. Calculation of supercritical flow over the tip region of a rotor blade at arbitrary azimuth. Paper presented at IMA Conference on numerical methods in applied Fluid Dynamics, Reading, 1978.

10 F X Caradonna, J J Philippe. The flow over a helicopter blade tip in the transonic regime. Proceedings of the 2nd European Rotorcraft and Powered Lift Aircraft Forum, September 1976.

11 B Monnerie, J J Philippe. Aerodynamic problems of helicopter blade tips. Proceedings of the 3rd European Rotorcraft and Powered Lift Aircraft Forum, Aix-en-Provence, September 1977.

12 J Grant. A method for the computation of steady or time-dependent two-dimensional supercritical flow about an aerofoil or an inboard section of a helicopter rotor blade. RAE Technical Report to be issued.

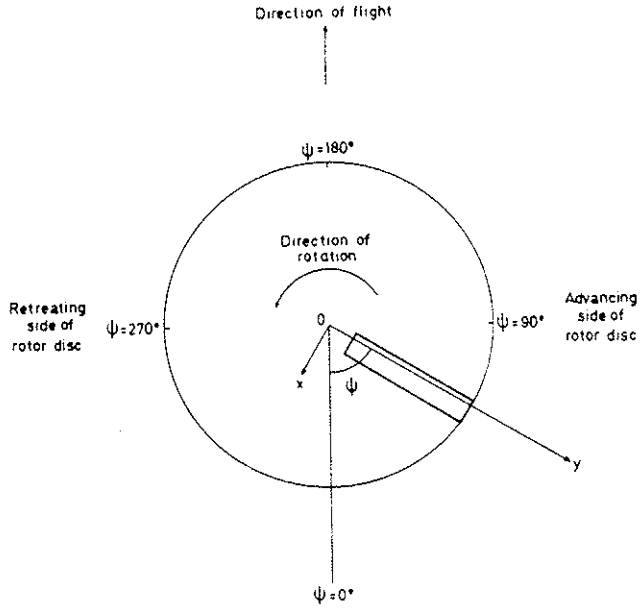


Fig 1 Definition of blade azimuth angle

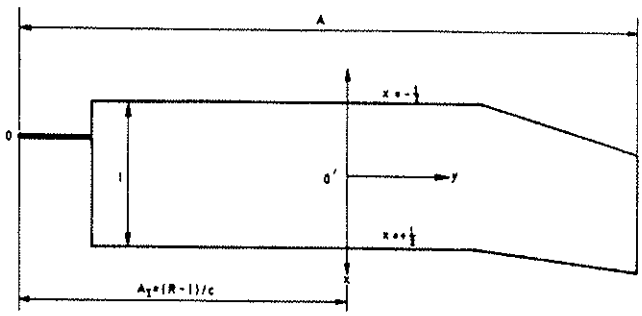


Fig 2 Typical rotor blade defining the independent variables x and y

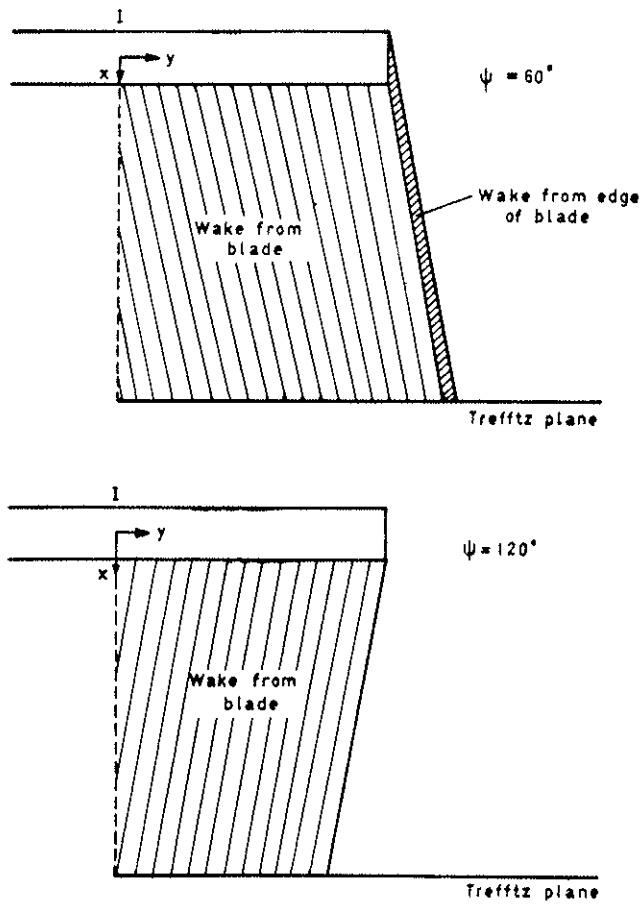


Fig 3 Model of wake at 60° and 120° azimuth

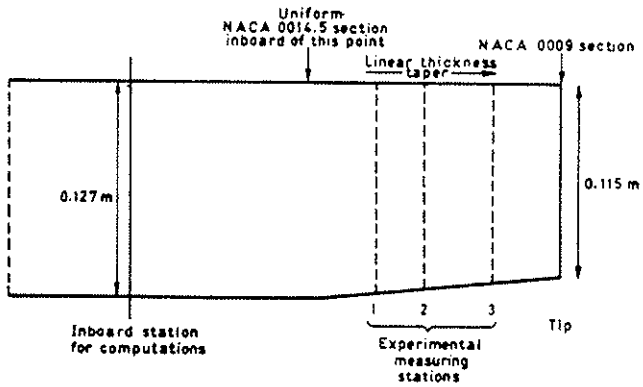


Blade chord c=0.127m, blade radius R=0.75m, A=5.9055

Fig 4 Geometry of ONERA near-rectangular tip

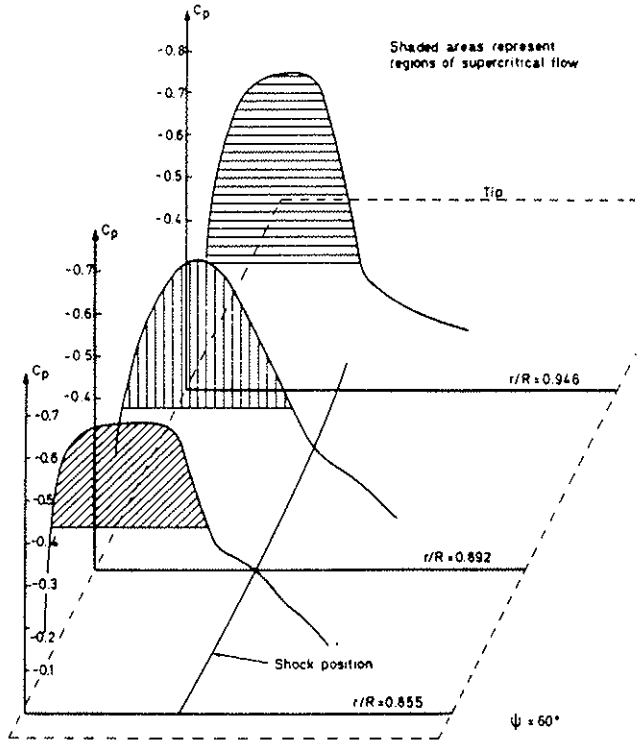


Fig 5 Measured three-dimensional pressure distribution on the blade tip at $\psi = 60°$, taken from Ref 6

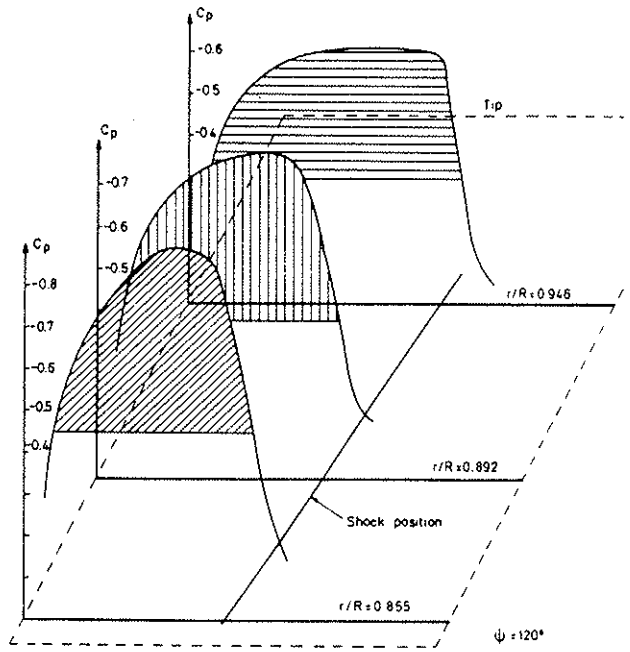


Fig 6 Measured three-dimensional pressure distribution on the blade tip at $\psi = 120°$

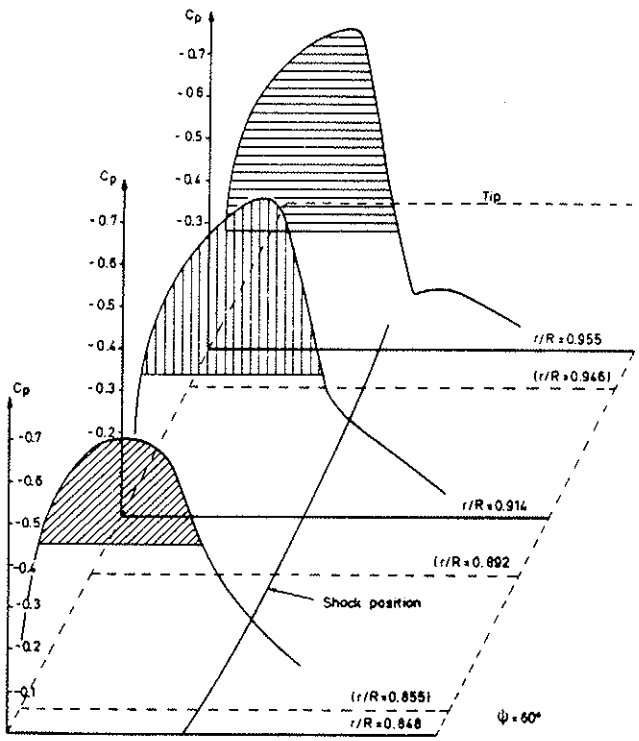


Fig 7 Calculated three-dimensional pressure distribution on the blade tip at $\psi = 60°$

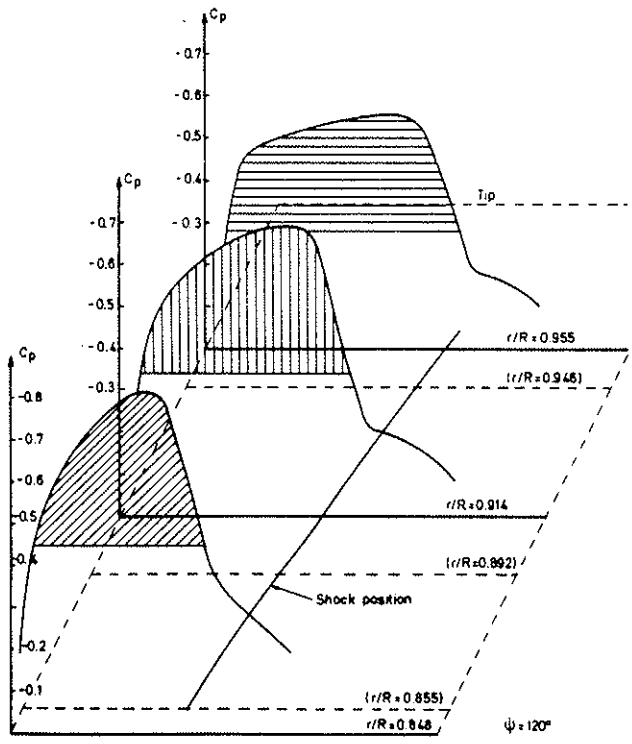


Fig 8 Calculated three-dimensional pressure distribution on the blade tip at $\psi = 120°$

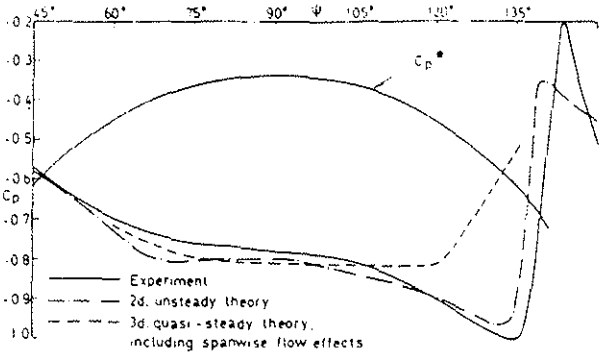


Fig 9a Measured and computed pressures at x/c = 0.3, r/R = 0.855

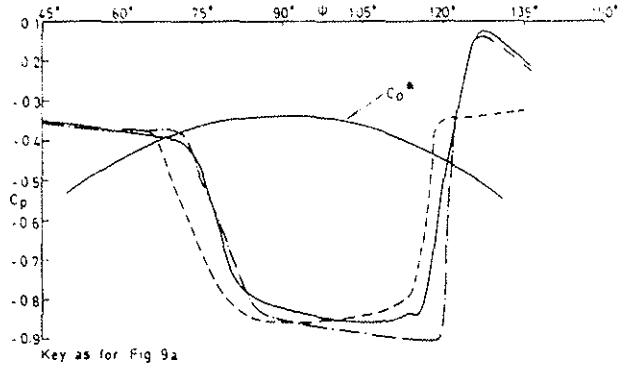


Fig 9b Measured and computed pressures at x/c = 0.5, r/R = 0.855

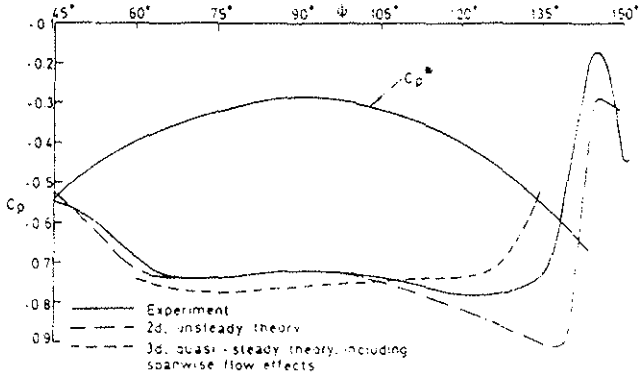


Fig 10a Measured and computed pressures at x/c = 0.30, r/R = 0.892

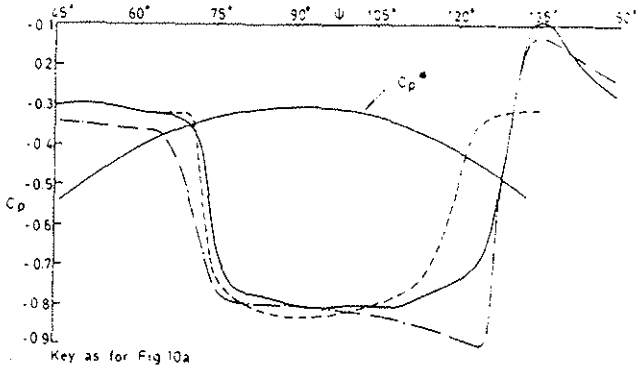


Fig 10b Measured and computed pressures at x/c = 0.50, r/R = 0.855

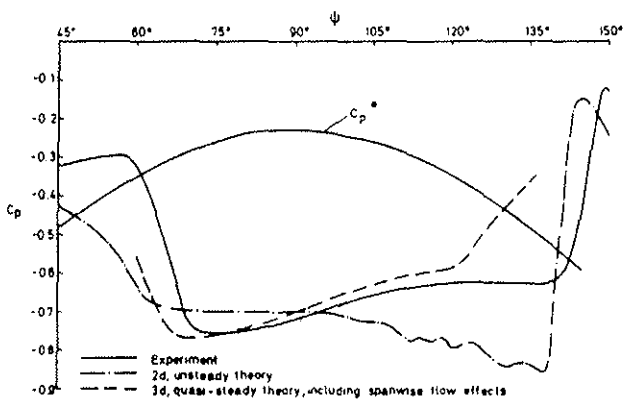


Fig 11 Measured and computed pressures at x/c = 0.40, r/R = 0.946

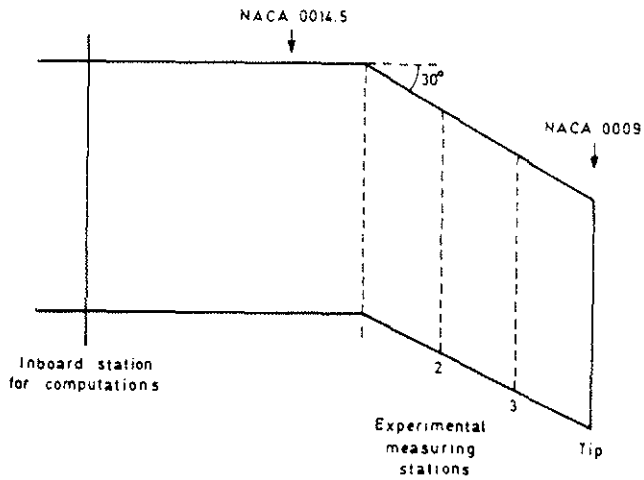


Fig 12 Geometry of ONERA swept-tip blade

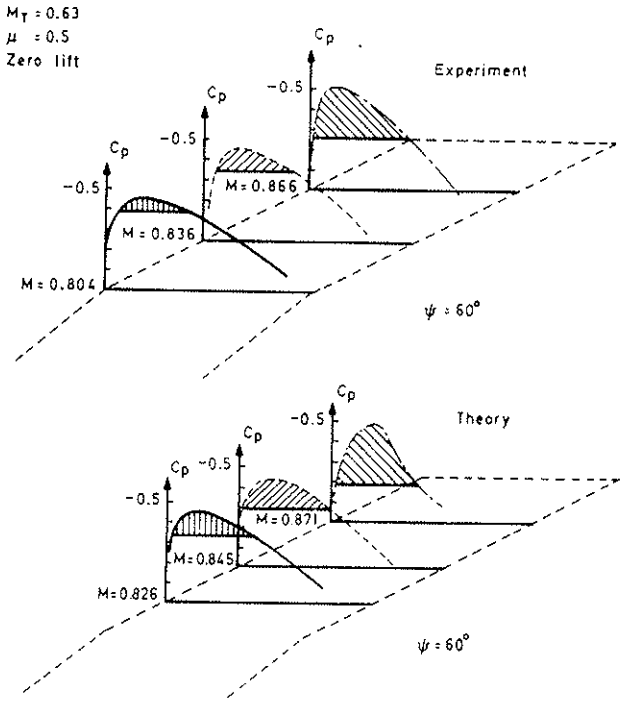


Fig 13 Three-dimensional pressure distributions on 30° swept-tip

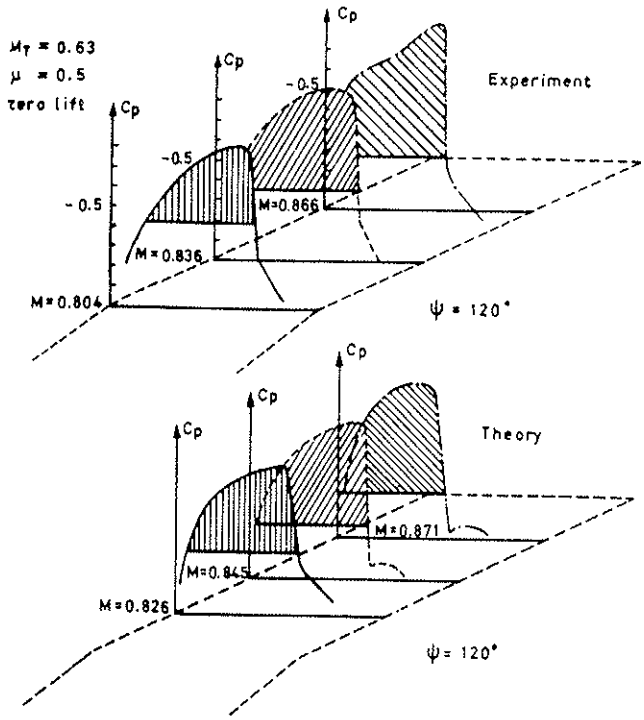


Fig 14 Three-dimensional pressure distributions on 30° swept-tip

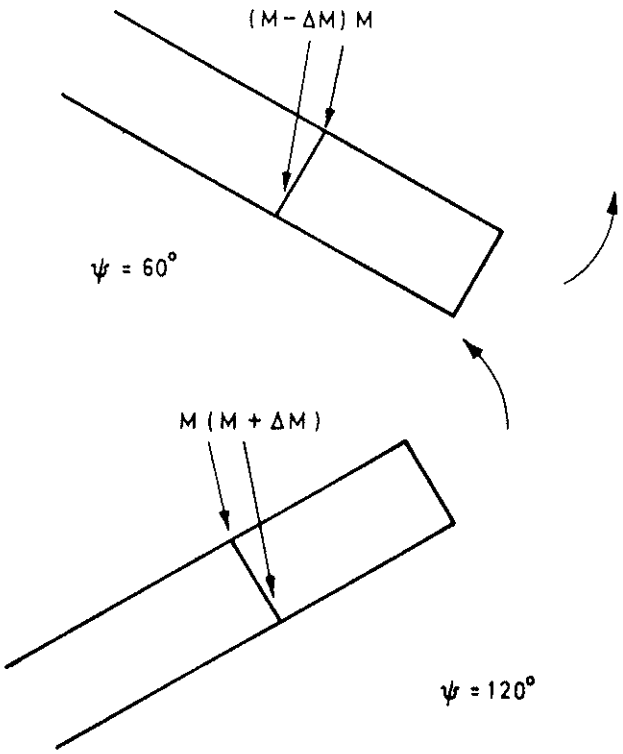


Fig 15 Effect of spanwise flow at 60° and 120° azimuth

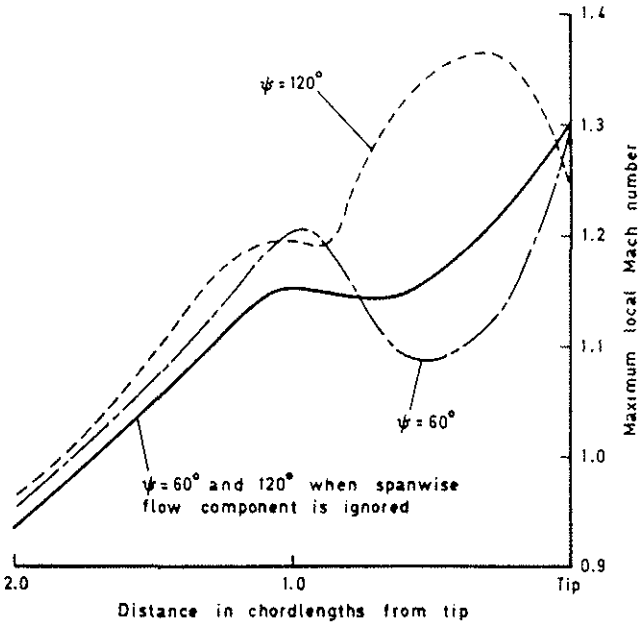


Fig 16 Calculated spanwise variation of maximum local Mach number for ONERA swept-tip

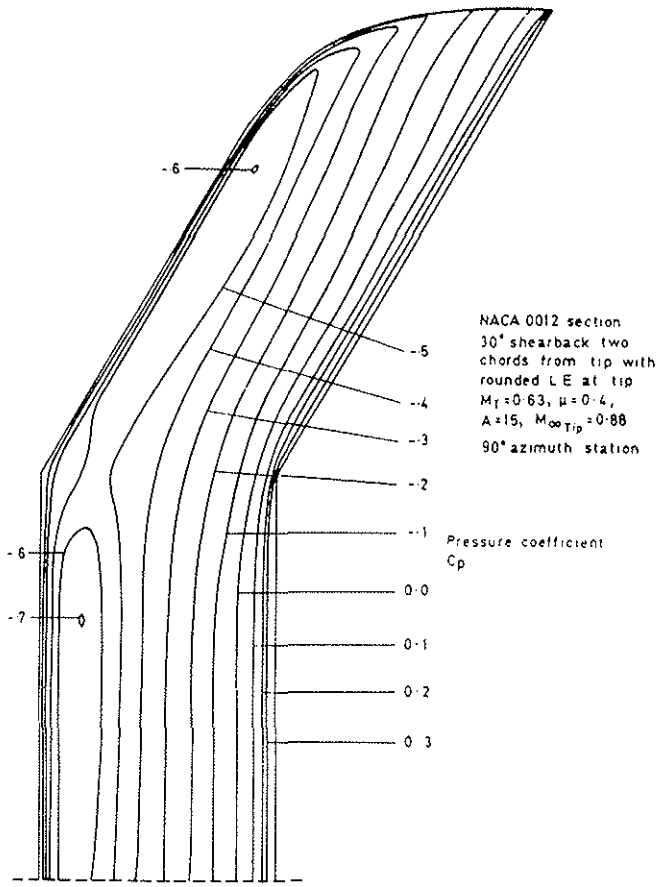


Fig 17 Isobar distribution for a 30° sheared blade with a rounded leading edge at the tip

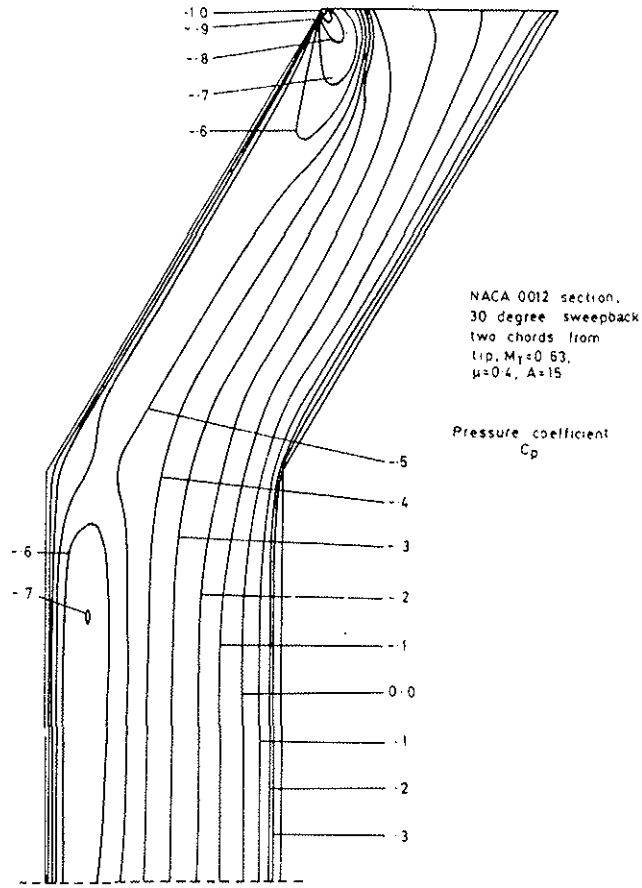


Fig 18 Isobar distribution for a blade sheared back sharply at 30° two chords from the tip

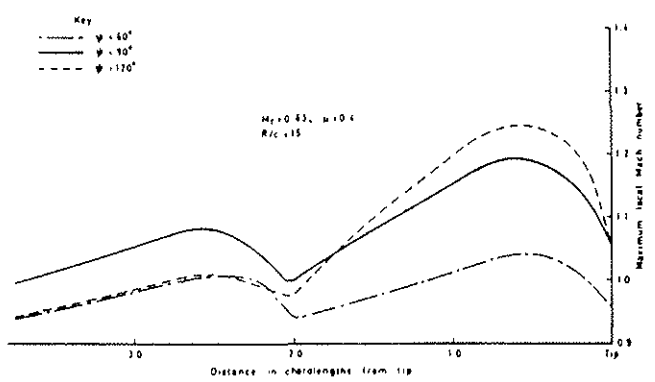


Fig 19 Calculated spanwise variation of maximum local Mach number for a sharply sheared tip

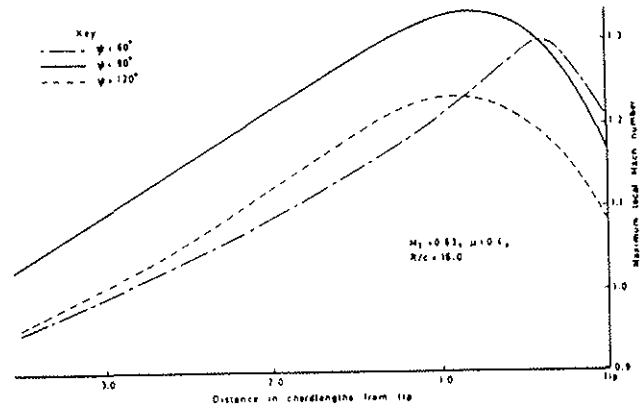


Fig 20 Calculated spanwise variation of maximum local Mach number for a rectangular tip

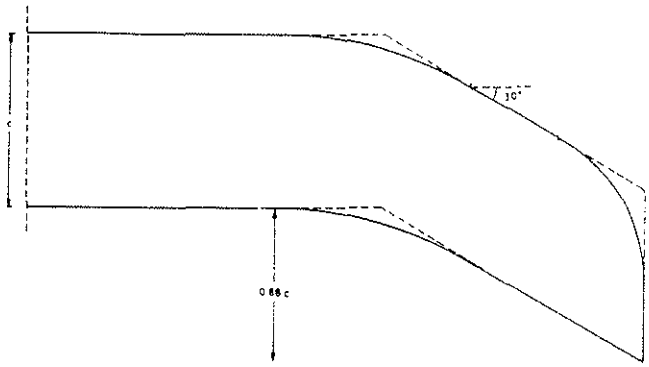


Fig 21 Improved design with progressive shearing

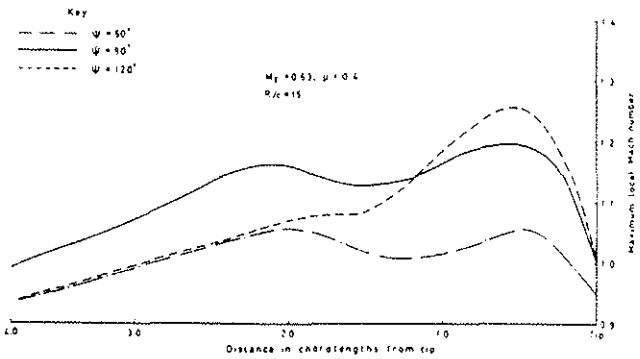


Fig 22 Calculated spanwise variation of maximum local Mach number for progressively sheared tip

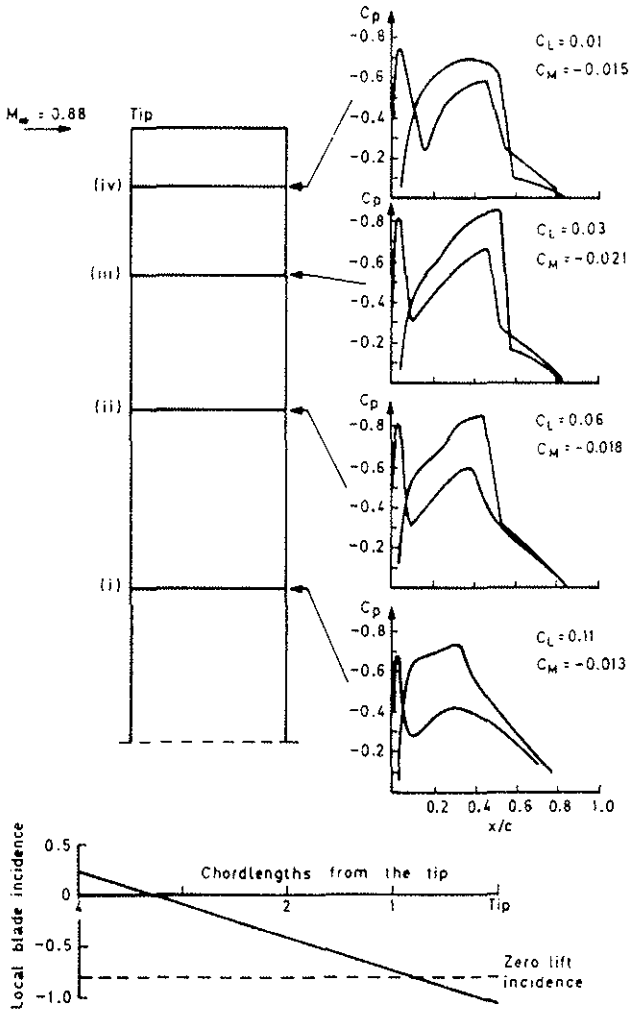


Fig 23 Calculated pressure distribution on a rectangular blade with 9615 section in lifting conditions